JOURNAL OF SOLID STATE CHEMISTRY **138,** 74–86 (1998)
ARTICLE NO. SC987756

New Phases Formed in the Li–Ti–O System under Reducing Conditions

I. E. Grey,* L. M. D. Cranswick,* C. Li,* L. A. Bursill,† and J. L. Peng†

*CSIRO Division of Minerals, Clayton, Victoria, 3168, Australia; and †University of Melbourne, School of Physics, Parkville, Victoria 3052, Australia

Received August 4, 1997; in revised form December 29, 1997; accepted January 8, 1998

Phase equilibria in the low-lithia (< 30 mole% Li_2O) part of the system Li_2O–TiO_2–Ti_2O_3 have been studied under reducing conditions established by H_2/CO_2 mixtures. At 1100° C and a H_2/CO_2 ratio of 70 ($fO_2 = 10^{-16.7}$ atm), the Li_2O–TiO_{2-X} join comprises alternating one- and two-phase regions in the range 30–6.5 mole% Li_2O. Single-phase regions occur at compositions centered at ~24 mole% Li_2O (ramsdellite-type, $Li_{2.2}Ti_{3.5}O_8$) and ~13 mole% Li_2O (1:1 ramsdellite:rutile ordered intergrowth, $Li_{0.9}Ti_{2.94}O$). By varying the temperature and H_2/CO_2 ratio, the intergrowth phase was prepared as a single phase in the range 12.8–14.5 mole% Li_2O. The intergrowth phase reacts readily with air, undergoing both oxidation of Ti^{3+} to Ti^{4+}, and hydroxylation/hydration of lithium in the structure to form $LiOH \cdot H_2O$. The reactions with air were quantified using weight gain experiments and Ti^{3+} analyses. The composition region from 6.5 to 0.7 mole% Li_2O is spanned by series of rutile-derived crystallographic shear (CS) structures. The CS plane orientation changes continuously with decreasing lithium content from $(051)_r$ to $(021)_r$. At less reducing conditions, the $(0kl)_r$ CS phases become unstable relative to a high-temperature, lithium-stabilized anatase phase containing ~4 mole% Li_2O. Powder X-ray, neutron, and electron diffraction techniques have been applied to determine and refine the structures of the different phases.

INTRODUCTION

Compounds in the Li_2O–TiO_2–Ti_2O_3 system are of interest to materials chemists because of their unusual physical properties and potential technological applications. The ramsdellite-related compound $Li_2Ti_3O_7$ has been the subject of numerous studies because of its high Li^+ ion conductivity (1). Lithium titanate spinels can undergo extensive and reversible lithium insertion/extraction with negligible changes to the unit cell dimensions, and so are well suited to advanced battery applications (2). The spinel $LiTi_2O_4$, containing both Ti^{3+} and Ti^{4+}, exhibits superconductivity below 13 K (3). The lithium titanates are also very useful starting materials for preparing new forms of titania by proton exchange and dehydration (4, 5).

Another interesting aspect of lithium compound chemistry relates to catalysis of gas–solid reactions, particularly the reduction of metal oxides with carbon. This has application to the commercial reduction of ilmenite, $FeTiO_3$. In Australia ilmenite is upgraded by the Becher process (6), which involves char reduction of ilmenite at ~1100–1150°C to produce metallic iron and titania-rich phases. The iron is removed by accelerated corrosion, giving a synthetic rutile product containing typically 92–94 wt% TiO_2 which is used as a feedstock for titania pigment production. Increasing the rate of the gasification reactions at the char surfaces in the reduction stage by catalysis has obvious benefits in terms of increased plant production or operation at lower temperatures. In a recent study, Mohanti and Smith (7) found that lithium carbonate was an effective catalyst for the reduction of ilmenite by carbon. They noted that sodium and potassium compounds were less effective catalysts and suggested that this was due to reaction with the ilmenite to form alkali titanates. They did not report on the reactions between lithia and the ilmenite.

As part of a general study on titanate chemistry related to ilmenite reduction, we investigated the low-lithia part of the Li_2O–TiO_{2-x} join using reduction conditions relevant to char reduction of ilmenite. Mixtures of hydrogen and carbon dioxide were used to establish the reducing atmospheres. The phases that formed in products obtained from equilibrations using varying Li:Ti ratios were characterized by a combination of chemical analyses, electron diffraction, and powder X-ray diffraction (PXRD). Structure determinations and refinements of new phases were made using PXRD data and neutron diffraction data. The results of these phase equilibria and structure characterization studies are reported here.

PREVIOUS STUDIES

The literature on compounds in the Li_2O–TiO_2–Ti_2O_3 system is extensive and includes studies on numerous metastable phases formed by insertion and exchange reactions at low temperatures. Here we consider only work related to

0022-4596/98 $25.00

the current study, concerning phases prepared at high temperatures in the low Li_2O (< 30 mole% Li_2O) region of the ternary system. The binary Li_2O–TiO_2 system was investigated by Izquierdo and West (8). The phases found in the low Li_2O region were a spinel phase, $Li_4Ti_5O_{12}$, stable up to 1015°C, and $Li_2Ti_3O_7$ with a ramsdellite-type structure. The phase relations of $Li_2Ti_3O_7$ were investigated in more detail by Mikkelson (9). $Li_2Ti_3O_3$ is stable from 940°C to its congruent melting point at 1300°C. Below 940°C it decomposes to $Li_4Ti_5O_{12}$ plus rutile. Mikkelsen identified a metastable hexagonal modification of $Li_2Ti_3O_7$ that formed below 940°C.

The structure of $Li_2O_3O_7$ was determined by Morosin and Mikkelsen (10). They reported the phase to be orthorhombic, *Pbnm*, with $a = 5.016(3)$, $b = 9.543(5)$, and $c = 2.945(2)$ Å. Their structure determination confirmed a ramsdellite-type (11) structure comprising double chains of edge-shared octahedra, which are corner-linked to give $[2 \times 1]$ channels along the chain direction. Morosin and Mikkelsen proposed that the lithium was distributed partly in the channels and partly in the octahedral framework, where it substituted for titanium, giving a unit-cell formula of $Li_{1.72}(Ti_{3.43}Li_{0.57})O_8$. The distribution of lithium over both octahedral and channel sites was confirmed by a later neutron diffraction study (12).

Phase and structure information on the ternary system has been recently reviewed by Strobel *et al.* (13). The only compounds containing both Ti^{3+} and Ti^{4+} that have been studied in detail are members of the spinel solid solution $Li_{1+x}Ti_{2-x}O_4$, $0 < x < 0.33$ (14), which are of particular interest because of their superconductivity and intercalation properties. Akimoto and coworkers (15–17) have prepared single crystals of various ternary phases by the reaction of metallic lithium with titanium oxides in a sealed iron container at temperatures in the range 1100–1200°C. In addition to spinel-type $LiTi_2O_4$ (15), they prepared the new phases $Li_{0.5}TiO_2$ (16) and $Li_{0.74}Ti_3O_6$ (17) and determined their crystal structures. $Li_{0.5}TiO_2$, with $Ti^{3+}/Ti^{4+} = 1$, has a ramsdellite-type structure. It differs from ramsdellite-type $Li_2Ti_3O_7$ in having lithium ordered only in the channels and not in the titanate framework. The phase $Li_{0.74}Ti_3O_6$, with $Ti^{3+}/Ti^{4+} = 0.33$, has monoclinic symmetry, $C2/m$, with $a = 14.120(1)$, $b = 2.949(1)$, $c = 4.973(1)$ Å, $\beta = 92.69(1)^\circ$ (17). Its structure can be described as an ordered 1:1 intergrowth, parallel to $(100)_r$ of rutile-type and ramsdellite-type structures. The lithium atoms are located in the ramsdellite-type channels with an occupancy factor of 0.37.

EXPERIMENTAL

Syntheses and Analyses

Starting materials for the synthesis experiments were AR grade TiO_2 (99.9% anatase form) and lithium carbonate. Mixtures corresponding to Li_2O contents in the range 0.7 to 30 mole% were carefully weighed, intimately ground together, and prereacted in air at 900°C to decompose the carbonate. The samples were pressed into pellets which were contained in molybdenum boats and heated in a tube furnace at 1100°C under a flowing reducing gas atmosphere established by mixing hydrogen and carbon dioxide. Each sample was given two preliminary heats for 4 h, with intermediate grinding and repelleting, followed by a third heat for typically 20 h. Many samples were given a second 20 h heat to ensure equilibrium was achieved. The samples were cooled rapidly in high-purity nitrogen and carefully weighed after each heat treatment to check for loss of lithium as volatile species. The majority of the equilibrations were made at 1100°C and at a H_2/CO_2 volume ratio of 70, since testwork showed that when ilmenite was reduced under these conditions the reduced products matched those obtained in Becher plants. Experiments were also conducted at 1000 and 1200°C with the H_2/CO_2 ratio fixed at 70, and at 1100°C with H_2/CO_2 ratios between 1 and 125.

Selected products were analyzed for Ti and Li using atomic emission spectroscopy (ICP-AES) to check that the ratios used in the starting mixtures were retained. Trivalent titanium was determined by dissolving the ground sample in a H_2SO_2/HF solution containing excess ferric iron, then titrating the ferrous iron formed ($Ti^{3+} + Fe^{3+} \rightarrow Ti^{4+} + Fe^{2+}$) against potassium dichromate. The method was calibrated using reduced titanium oxides of known composition. From testwork it was confirmed that lithium did not interfere with the trivalent titanium analyses.

Diffraction Studies

PXRD was used for the routine identification of phases in the equilibrated products and to provide intensity data for structure refinements by the Rietveld method (18). Samples for PXRD were prepared by grinding the reaction pellets in a tungsten carbide mill and back-pressing the powders into an aluminum sample holder. Measurements of diffracted intensities were made using a Philips 1050 goniometer with a PW1710 controller and a long, fine-focus copper tube operated at 40 kV and 40 mA. The diffractometer was configured with a 1° divergent slit, 0.2 mm receiving slit, 1° scatter slit, incident and diffracted beam Soller slits, and a diffracted-beam curved graphite monochromator.

Electron diffraction/microscopy studies were made using a JEOL-4000EX high resolution transmission electron microscope operated at 400 kV. Studies were made on thin edges of crystals produced by fracturing.

The powder neutron diffraction (PND) data collection was made on a cylindrical specimen composed of 1 cm diameter pressed pellets, and weighing ~ 6 g. The sample was contained in a vanadium can. The data set was collected on the high-resolution powder diffractometer at the Australian Nuclear Science and Technology Organisation's

research reactor. Intensity data was collected in the 2θ range 0.08–154.08°, at intervals of 0.05°, using a wavelength of 1.3717 Å and a total counting time of 24 h.

Rietveld Refinements

For the Rietveld refinements, intensity data were collected on hand-ground samples at 22°C, from 10° to 140° 2θ with a step size of 0.025° and a counting time of typically 4 sec/step.

Least squares refinements were carried out using the Rietveld program SR5, a local modification of the code by Hill & Howard (19) and Wiles & Young (20) which allows for quantitative phase analysis of multi-phase mixtures. Profile refinement parameters included a scale factor, two pseudoVoigt shape parameters, a 2θ zero parameter, a three-term full-width at half-maximum function (21), calculated for nine half-widths on either side of the peak maxima, a peak asymmetry parameter for peaks less than 50° 2θ, and unit cell parameters. The background was modeled using a five-parameter polynomial fit. Scattering curves for neutral atoms were taken from International Tables for X-ray Crystallography (22). For the PND refinement a Voigt shape function was used.

Structure Determination of the 1 : 1 Intergrowth Phase

At the time this study was conducted, the structure of the 1:1 ramsdellite-rutile intergrowth phase had not been reported (17). An *ab initio* structure determination was undertaken for this phase using PXRD data. The positions of 27 nonoverlapping peaks were measured off the PXRD pattern for the sample containing 14.6 mole% Li_2O and used in ITO (23) to determine and refine the unit cell. With the assistance of the determined cell parameters, the powder pattern was decomposed using the Philips APD program to obtain the intensities of 47 reflections out to $2\theta = 65°$. The intensities were corrected for multiplicity and converted to structure factors. These were used in SHELX-76 (24) to generate a Patterson map, which was solved for the positions of the titanium atoms. The oxygen atoms were located in difference Fourier maps. The structure was then refined using the Rietveld method. Refinement of 31 profile parameters, atomic coordinates, and isotropic displacement parameters converged at $R_{wp} = 0.16$, $R_B = 0.073$. Attempts to locate the lithium atoms using difference Fourier maps were not successful.

To assist in the location of the lithium atoms, a powder neutron diffraction data set was collected and refined, using the atomic coordinates obtained from the PXRD refinement as starting values. The Rietveld refinement proceeded smoothly, and a difference Fourier map revealed the position of lithium atom in the ramsdellite-type $[2 \times 1]$ channel. This was included in the refinement and its site occupation factor was refined. In the final refinement, 47 profile, positional, and isotropic displacement parameters were refined, resulting in convergence at $R_{wp} = 0.073$, $R_B = 0.041$.

RESULTS AND DISCUSSION

Phase Studies

The Li_2O–TiO_{2-x} Pseudobinary Join at 1100°C and $10^{-16.7}$ atm

The results of phase equilibria studies at 1100°C using a H_2/CO_2 ratio of 70 ($fO_2 = 10^{-16.7}$ atm), for Li_2O contents in the range 0–30 mole% are given in Table 1. The results are presented schematically in Fig. 1. In summary, the Li_2O–TiO_{2-x} join comprises alternating one- and two-phase regions in the range 30–6.5 mole% Li_2O, with the single-phase regions occurring at Li_2O compositions centered at 24 mole% and 13 mole% Li_2O. From 6.5 to 0.7 mole% Li_2O, the composition region is quasi-single phase but with a different structure at each point. The different phase regions will be considered below in order of decreasing Li_2O content.

TABLE 1
Equilibrations at 1100°C, $fO_2 = 10^{-16.7}$ atm

Mole% Li_2O in starting mixture	Phases in equilibrated products	Wt% Ti_2O_3 in product
25	ramsdellite-type (dominant) + rock-salt-type (trace)	
24	ramsdellite-type	11.6
23	ramsdellite-type (dominant) + 1:1 intergrowth (trace)	
14.5	1:1 intergrowth (dominant) + ramsdellite (trace)	
14.1	as above, less ramsdellite	
13.7	1:1 intergrowth	19.4
13.1	1:1 intergrowth	
12.8	1:1 intergrowth	18.5
12.3	1:1 intergrowth (major) + $(0kl)_r$ CS (minor)	
8.0	1:1 intergrowth + $(0kl)_r$ CS	
7.6	$(0kl)_r$ CS (major) + 1:1 intergrowth (minor)	
7.1	$(0kl)_r$ CS (dominant) + 1:1 intergrowth (trace)	
6.5	$(0kl)_r$ CS	17.9
5.2	$(0kl)_r$ CS	17.2
3.6	$(0kl)_r$ CS	
2.6	$(0kl)_r$ CS	13.8
1.3	$(0kl)_r$ CS	
0.7	$(0kl)_r$ CS (dominant) + $(132)_r$ CS	8.3
0.0	$(132)_r$ CS	6.1

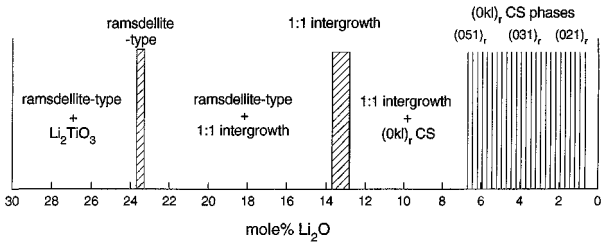

FIG. 1. Phase relations for the pseudobinary join Li_2O–TiO_{2-x}, at 1100°C and $fO_2 = 10^{-16.7}$ atm.

23–25 mole% Li_2O. A ramsdellite-type phase was found to occupy a narrow composition interval centered near 24 mole% Li_2O. At 25 mole% Li_2O, a cubic rock salt-type phase, $\sim Li_2TiO_3$, was present as a minor second phase, while at a composition of 23 mole% Li_2O, a ramsdellite-rutile ordered intergrowth phase containing 13.7 mole% Li_2O was present as a minor phase. The single phase composition of 24 mole% Li_2O has an atomic fraction of lithium, [Li] / [Li + Ti], of 0.39, which is between the values of 0.4 for $Li_2Ti_3O_7$ (10) and 0.33 for ramsdellite-type $Li_{0.5}TiO_2$ (16). From the Ti_2O_3 analysis of 6.2 wt% the unit cell composition can be calculated, giving $Li_{2.2}Ti_{3.5}O_8$. By analogy with $Li_2Ti_3O_7$ this can be written as $Li_{1.7}[Ti_{3.5}Li_{0.5}]O_8$, indicating that 12.5% of the octahedral sites in the ramsdellite framework are occupied by lithium. The orthorhombic unit cell parameters obtained from a Rietveld refinement are $a = 5.0138(4)$, $b = 9.5527(7)$, and $c = 2.9481(4)$ Å.

12.8–13.7 mole% Li_2O. A phase with monoclinic symmetry, related to the recently reported 1 : 1 ramsdellite-rutile intergrowth compound (17), was found to be stable in the composition range from 12.8 to 13.7 wt% Li_2O. Powdered samples of the intergrowth phase were unstable in air, reacting readily with moisture in the air to form $LiOH \cdot H_2O$ and a lithium-depleted intergrowth phase as will be discussed below. When proper care was taken to analyze fresh samples in a moisture-free environment, values of 18.5 and 19.4 wt% Ti_2O_3 were obtained for single-phase samples corresponding to 12.8 and 13.7 mole% Li_2O, respectively. The resulting calculated compositions normalized to six oxygen are $Li_{0.86}Ti_{2.94}O_6$ and $Li_{0.93}Ti_{2.93}O_6$, respectively. These compare with the composition $Li_{0.74}Ti_3O_6$ prepared by Akimoto *et al.* (17) by reaction of metallic lithium and titanium oxide in a sealed container. Rietveld refinement of the PXRD pattern for $Li_{0.93}Ti_{2.93}O_6$ gave the monoclinic unit cell parameters $a = 4.9253(2)$, $b = 14.1046(6)$, $c = 2.9501(1)$ Å, and $\gamma = 92.270(2)^\circ$. The space group setting $A112/m$ has been chosen so that the unit cell parameters are oriented in the same way as in the ramsdellite and rutile component structures.

0–6.5 wt% Li_2O. At Li_2O contents between 13.7 and 6.5 mole% the 1 : 1 intergrowth phase coexists with a new phase having a rutile-related PXRD pattern. The diffractogram for the 6.5 mole% Li_2O phase resembles patterns obtained for high-temperature rutile-related crystallographic shear (CS) structures in the Fe_2O_3–TiO_2 system (25). Between 6.5 and 0.7 mole% Li_2O, each composition gave a different but related single-phase PXRD pattern. The PXRD patterns of three different compositions with Li_2O contents of 6.4, 2.6, and 1.3 mole% Li_2O are compared with that for rutile in Fig. 2. It is seen that some rutile subcell reflections are retained in the new phases and their positions remain almost unchanged with composition, whereas other rutile subcell reflections are split into satellites showing large movements as a function of composition.

Further information on the nature of the rutile-related CS phases was obtained from electron diffraction studies. These

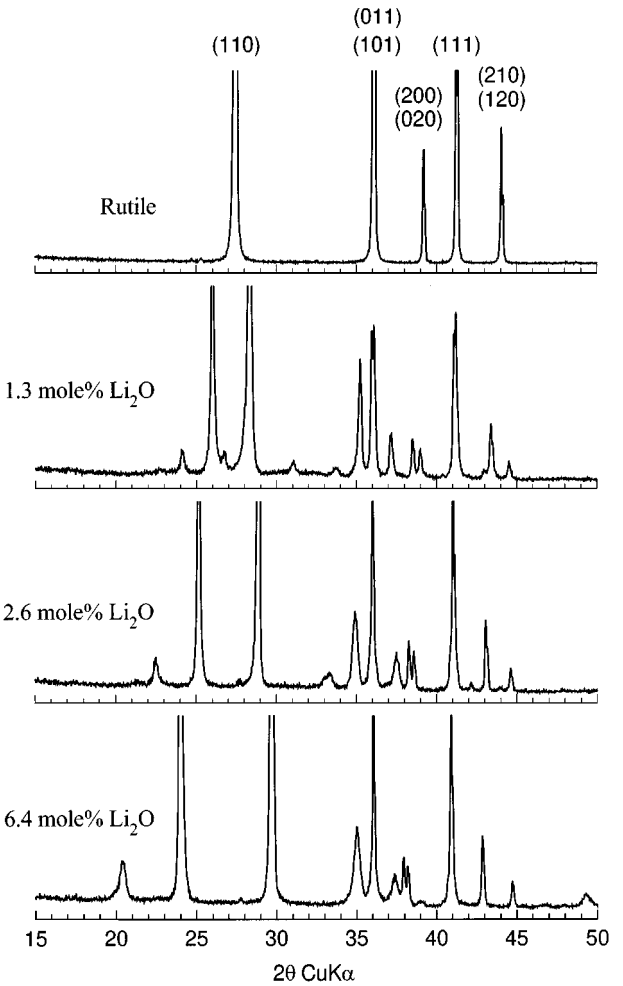

FIG. 2. Powder X-ray diffractograms of $(0kl)_r$ CS phases, compared with rutile (upper diffractogram). Rutile subcell reflections $(011)_r$ and $(111)_r$ are seen to be unchanged in the CS phases, whereas the other subcell reflections are split into satellites.

showed rows of superlattice reflections that were oriented in $[100]_r$ zone patterns. At the upper composition limit of 6.5 mole% Li_2O, the superlattice rows were oriented along $\mathbf{g}(051)_r$. With the progressive decrease in Li_2O content, the superlattice rows rotated away from $\mathbf{g}(051)_r$ toward $\mathbf{g}(021)_r$. This is illustrated in the $[100]_r$ zone axis electron diffraction patterns shown in Fig. 3 for compositions containing 6.4 and 0.7 mole% Li_2O. In the 6.4 mole% Li_2O sample the superlattice rows are oriented close to $\mathbf{g}(051)_r$, while at 0.7 mole% Li_2O the direction of the superlattice rows has swung around to $\mathbf{g}(021)_r$. Zone axis photos taken perpendicular to the $[100]_r$ zone confirm that there is no swinging of the CS planes out of the $[001]_r$ zone, for example as shown for the $[001]_r$ zone in Fig. 4.

The CS planes corresponding to the observed range of superlattice directions can all be described by the general

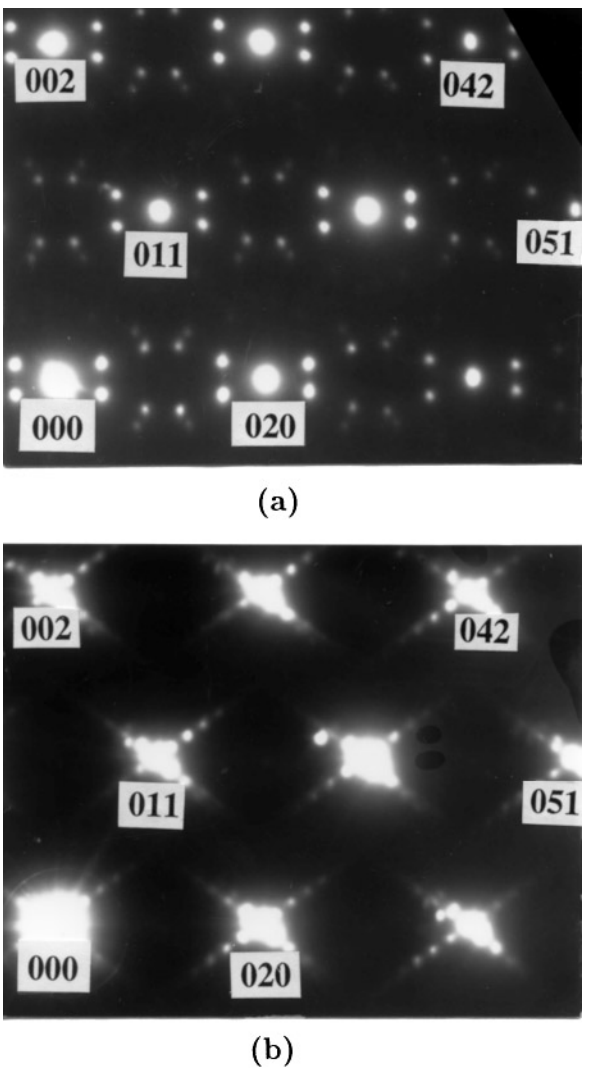

FIG. 3. $[100]_r$ zone axis electron diffraction patterns for $(0kl)_r$ CS phases with (a) 6.5 mole% Li_2O and (b) 0.7 mole% Li_2O.

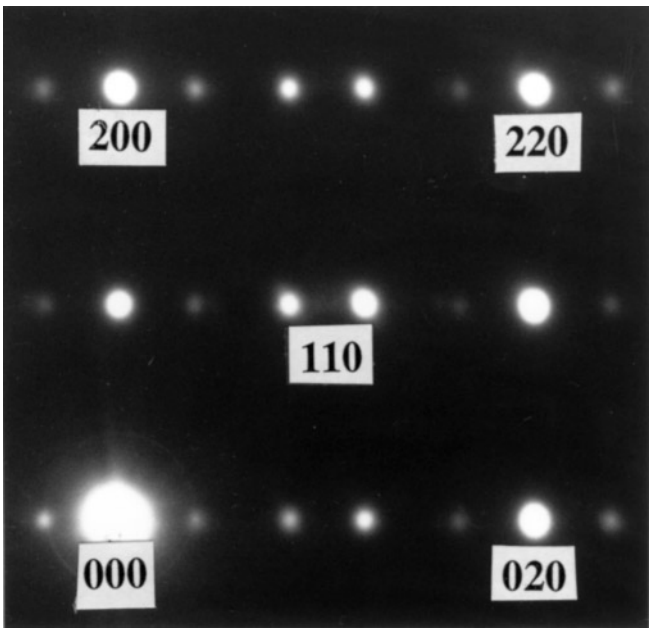

FIG. 4. $[001]_r$ zone axis electron diffraction pattern for $(051)_r$ CS phase.

expression

$$(0kl) = p\cdot(020)_r + q\cdot(011)_r,$$

where p and q are integers. Although end-member $(020)_r$ CS structures were not formed in the Li_2O–TiO_{2-x} system under the conditions used, we prepared $(020)_r$ phases by reacting ilmenite with Li_2O under similar reducing conditions.

The expression given above is the same as that used to describe the observed CS behavior in the TiO_2 + 8–13 wt% Fe_2O_3 system (25). In the iron-doped system the $(0kl)_r$ CS phases were stable only at temperatures above 1450°C, close to the melting point of the phases. The phases had to be quenched to avoid their transformation into $(121)_r$–$(132)_r$ CS structures that are stable at lower temperatures, and this made it difficult to obtain well-ordered samples. The problem of long-range ordering in the iron-doped samples was exacerbated by the relatively large separations between the CS planes, typically 25–30 Å. In contrast, the lithium-doped samples are stable at lower temperatures and the atomic order is quite well developed as shown in Fig. 3, where up to four orders of satellite reflections are visible.

The PXRD pattern for the composition containing 0.7 mole% Li_2O showed extra weak peaks consistent with the presence of a small amount of a $(132)_r$ CS structure, thus defining the limit for the $(0kl)_r$ CS structures. A lithium-free composition equilibrated at the same conditions as the lithium-doped samples was analyzed as $TiO_{1.96}$. Electron diffraction patterns showed that the CS plane orientation

was $(132)_r$, with 32–34 superlattice spots out to $\mathbf{g}(132)_r$. The observed satellite spacing can also be used to calculate a composition close to $TiO_{1.96}$.

Studies at Various Temperatures and Reducing Atmospheres

Selected compositions were equilibrated at various temperatures with the H_2/CO_2 ratio fixed at 70, and also at various H_2/CO_2 ratios for a fixed temperature of 1100°C. The results are summarized in Table 2.

From Table 2 it is seen that the stability field for the 1:1 intergrowth phase could be extended to 14.5 mole% Li_2O at 1100 °C by increasing the oxygen fugacity to $10^{-15.0}$ atm, i.e., by using less reducing conditions. The analyzed trivalent titanium content, 14.7 wt% Ti_2O_3, was considerably lower in this sample than in the samples prepared at an oxygen fugacity of $10^{-16.7}$ atm. The calculated composition is $Li_{0.98}Ti_{2.88}O_6$. A comparison with the compositions obtained at $fO2 = 10^{-16.7}$ atm (given above) and with the composition of $Li_{0.74}Ti_3O_6$ obtained under strongly reducing conditions (17) shows that with decreasing trivalent titanium contents, the Ti/O atomic ratio progressively decreases below the value of 0.5 required for the octahedral framework. By analogy with the ramsdellite-related $Li_2Ti_3O_7$ compound, this indicates progressive substitution of lithium into the octahedral framework as the preparative conditions become less reducing.

The intergrowth phase stability field could be extended to 14.5 mole% Li_2O by the alternative preparative procedure of maintaining the H_2/CO_2 ratio at 70 and decreasing the temperature to 1000 °C. This is another means of obtaining less-reducing conditions. When the H_2/CO_2 ratio was decreased below 10 at 1100°C, the 1:1 intergrowth phase decomposed to a mixture of the ramsdellite-type phase plus rutile. Attempts to extend the stability field for the intergrowth phase to lower Li_2O contents by increasing the reducing conditions were not successful. As seen from Table 2, decreasing the oxygen fugacity to $10^{-17.3}$ atm at 1100°C, or increasing the temperature to 1200°C did not produce a pure intergrowth phase at Li_2O contents less than 12.8 mole%.

The effect of temperature variation on the $(0kl)_r$ CS phases was studied at temperatures of 1000 and 1200 °C, maintaining the H_2/CO_2 ratio fixed at 70. The CS phases remained stable at 1200 °C, but were unstable relative to a lithium-containing anatase phase at 1000 °C. The Li-anatase had a narrow compositional field of stability, close to 4 mole% Li_2O. Compositions with higher lithia contents gave two phase mixtures of Li-anatase and the 1:1 intergrowth phase, while compositions lower in lithia content gave rutile as a second phase. The Li-anatase was also formed at 1100 °C

TABLE 2
Equilibrations at Varying Temperatures and Reducing Atmospheres

Mole% Li_2O in starting mixture	Temp. (°C)	H_2/CO_2	log fO_2	Phases present (by XRD)
14.5	1100	1	− 13.0	ramsdellite-type + rutile
14.5	1100	5	− 14.4	as above
14.5	1100	10	− 15.0	1:1 intergrowth
14.5	1100	13	− 15.3	1:1 intergrowth (major) + ramsdellite-type (minor)
12.3	1100	40	− 16.3	1:1 intergrowth (major) + $(0kl)_r$ CS (minor)
12.3	1100	70	− 16.7	as above, less CS phase
12.3	1100	125	− 17.3	as above, less CS phase
6.5	1100	12	− 15.2	Li-anatase (major) + 1:1 intergrowth (minor)
6.5	1100	70	− 16.7	$(0kl)_r$ CS
14.5	1200	70	− 15.6	1:1 intergrowth (major) + ramsdellite-type (minor)
12.3	1200	70	− 15.6	1:1 intergrowth (major) + $(0kl)_r$ CS (minor)
7.6	1200	70	− 15.6	$(0kl)_r$ CS
3.6	1200	70	− 15.6	$(0kl)_r$ CS, 19.5 wt% Ti_2O_3
24.0	1000	70	− 18.3	ramsdellite-type
14.5	1000	70	− 18.3	1:1 intergrowth
12.3	1000	70	− 18.3	1:1 intergrowth (dominant) + anatase (trace)
5.2	1000	70	− 18.3	Li-anatase (major) + 1:1 intergrowth (minor)
4.0	1000	70	− 18.3	Li-anatase
2.6	1000	70	− 18.3	Li-anatase (major) + rutile (minor)

by increasing the oxygen fugacity to $10^{-15.2}$ atm, as shown in Table 2.

Extensive incorporation of lithium into the anatase structure has been previously reported using insertion methods at room temperature, but the results reported here appear to be the first published example of stabilization of anatase by lithium at high temperature. Evidently, trivalent titanium plays an important role in the stabilization, because rutile is the only TiO_2 polymorph that forms in the Li_2O–TiO_2 system at elevated temperatures.

Reaction of the 1 : 1 Intergrowth Phase with Air

Ground samples of the 1 : 1 intergrowth phase were observed to react readily with oxygen and moisture at ambient temperature, resulting in oxidation of the trivalent titanium and rejection of lithium from the structure as a hydrated hydroxide. Formation of $LiOH \cdot H_2O$ (26) as the hydration product was confirmed from PXRD patterns of the reacted samples. The reaction with air results in a change in colour from black to light grey, accompanied by a weight gain, a decrease in the analyzed Ti_2O_3 content, and changes to the cell parameters. The driving force for the reaction with air was determined to be the hydration step. Ground samples that were exposed to air from which the moisture had been removed using molecular sieves showed no reaction over extended periods. Thus in the absence of water vapor to react with the lithium, the intergrowth phase remains stable against air oxidation.

The initial rate of reaction was found to be directly related to the surface area of the ground samples. Ball-milled samples initially reacted more than twice as fast as hand-ground specimens. However after about one day the reaction rates approached a common value. These observations are qualitatively in accord with a topotactic reaction that is initially chemically controlled but then becomes diffusion controlled as a product layer develops.

Data from air reactions of two intergrowth phases containing 12.8 and 14.5 mole% Li_2O are given in Table 3. The phase containing 12.8 mole% Li_2O was split into two samples which were ball-milled and hand-ground respectively. From the Ti_2O_3 analyses of the air-reacted products, the weight gain due to oxidation was calculated and subtracted from the total weight gain, giving the weight gain due to hydration. It is seen from the results in Table 3 that the ratio of the hydration weight gain to oxidation weight gain is the same (3) for the two subsamples of the 12.8 mole% Li_2O composition. The composition with 14.5 mole% Li_2O has a higher ratio of hydration weight gain to oxidation weight gain, consistent with the lower Ti^{3+}/Ti^{4+} ratio in this sample.

Using the measured weight gains and Ti_2O_3 analyses in Table 3, equations for the reactions with moist air can be calculated. For example, for the ball-milled sample containing 12.8 mole% Li_2O, the reaction is:

$$Li_{0.86}Ti_{2.94}O_6 + 0.72H_2O + 0.12O_2 \rightarrow Li_{0.38}Ti_{2.94}O_6 + 0.48LiOH.H_2O.$$

TABLE 3
Reaction of 1 : 1 Intergrowth Phases with Air

Prep. Conditions	12.8 mole% Li_2O, 1100°C, $fO_2 = 10^{-16.7}$ atm			14.5 mole% Li_2O, $fO_2 = 10^{-15.2}$ atm	
Sample	fresh sample	hand ground	ball milled	fresh sample	hand ground
Exposure to air	none	8 days	8 days	none	7 days
% wt. gain	0.0	4.1	6.7	0.0	4.6
% Ti_2O_3	18.5	9.2	3.8	14.7	9.9
% wt. gain from oxidation		1.0	1.6		0.5
% wt. gain from hydration		3.1	5.1		4.1
Cell parameters					
a (Å)	4.9067(2)	4.8246(6)	4.7535(6)	4.9161(1)	4.8917(3)
b (Å)	14.107(1)	14.154(1)	14.147(1)	14.0970(4)	14.096(1)
c (Å)	2.9525(1)	2.9554(2)	2.9572(2)	2.9508(1)	2.9524(1)
γ (°)	92.234(3)	91.631(4)	91.844(4)	92.252(2)	92.172(3)
Parameters after long exposure			1 month		4 months
a (Å)			4.5968(8)		4.7455(2)
b (Å)			14.378(2)		14.1805(6)
c (Å)			2.9255(4)		2.9558(2)
γ (°)			90.00		91.464(2)

The proposed reaction involves hydroxylation and removal of lithium, and oxidation of trivalent titanium. It is consistent with the analytical measurements and the observed formation of $LiOH \cdot H_2O$ as a reaction product. Alternative reactions can be proposed, for example involving proton exchange for lithium in the intergrowth structure. A detailed study involving spectroscopic and thermal analysis methods would be required to confirm the correct mechanism.

The extent of reaction was found to be greater at the low-Li_2O end of the single phase region. This is illustrated in Table 3 by a comparison of the changes to the cell parameters on prolonged reaction of samples containing 12.8 and 14.5 mole% Li_2O. For the 14.5 mole% Li_2O sample, 4 months of exposure to air resulted in a 3% contraction in *a*, a 0.6% expansion in *b*, and a small decrease in the monoclinic angle. In contrast the unit cell for the 12.8 mole% Li_2O sample became orthorhombic, at least metrically, in less than a month. Relative to the starting material, the *a* parameter decreased by 6% and the *b* parameter increased by 2%. The PXRD pattern of the transformed 12.8 mole% Li_2O phase is compared with the pattern of the starting compound in Fig. 5. The presence of well-crystallized $LiOH \cdot H_2O$ in the pattern of the reacted phase is indicated by the arrows in Fig. 5.

Akimoto *et al.* (4) have reported a similar propensity for the ramsdellite-type phase, $Li_{0.5}TiO_2$, to oxidize at room temperature and lose lithium from the structure. The oxidation is accompanied by a contraction in the *b*-axis. This is in contrast to the behavior observed for the 1:1 intergrowth phase, for which *b* expands on reaction with air. Thermal analyses and spectroscopic measurements on the oxidation products of $Li_{0.5}TiO_2$ showed no evidence for protonation (4). The *a*-axis of the oxidized samples underwent only minor changes, even with complete removal of lithium, in contrast to the parameter changes accompanying oxidation/hydration of the 1:1 intergrowth phases in our study.

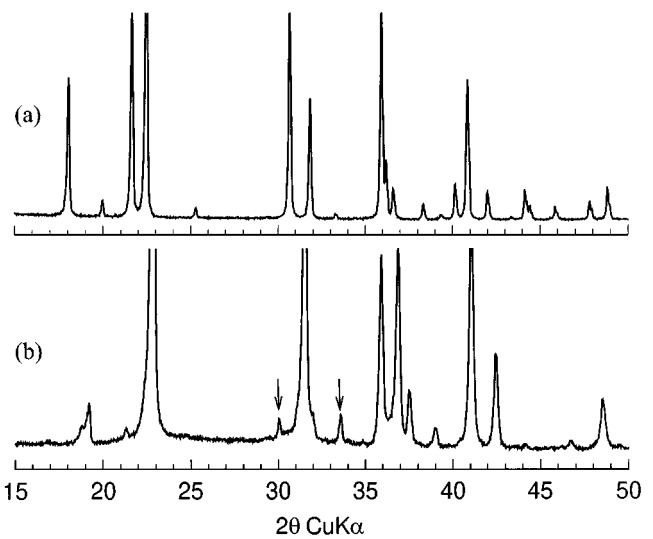

FIG. 5. Powder X-ray diffractograms for 1:1 ramsdellite:rutile intergrowth phases: (a) $Li_{0.98}Ti_{2.88}O_6$; (b) $Li_{0.86}Ti_{2.94}O_6$ after 1 month exposure to air. Arrows indicate peaks for $LiOH \cdot H_2O$.

A comparison of compositions and unit cell parameters for different ramsdellite-type and ramsdellite-rutile intergrowths in the Li–Ti–O system and their oxidation/leaching products in given in Table 4. The compositions reported in the literature are presented in different ways, often without a clear relationship to the structural formulae, for example $Li_2Ti_3O_7$ is commonly reported for a ramsdellite-type phase that actually contains eight oxygen atoms per unit cell. For consistency, in Table 4 the unit cell compositions are given in addition to the more commonly reported phase compositions. The unit cell parameters for the intergrowth phases have been reoriented from the reported $C12/m1$ space group setting (17) to the setting $A112/m$. This allows the relationships between the cells for rutile, ramsdellite, and the 1:1 intergrowth structure to be easily visualized. viz: a(rutile) $\equiv$ a(ramsdellite) $\equiv$ a(intergrowth), c(rutile) $\equiv$ c(ramsdellite) $\equiv$ c(intergrowth), and b(intergrowth) = b(rutile) + b(ramsdellite). Similarly the unit cell composition of the intergrowth phase is simply the sum of the unit cell compositions for rutile and ramsdellite-types.

Structure Studies

1 : 1 Rutile : Ramsdellite Intergrowth Structure

The results from the Rietveld refinement of the powder neutron diffraction data for the intergrowth phase, $Li_{0.98}Ti_{2.88}O_6$, are reported in Table 5. The positional parameters, including those for the lithium atom, are close to values recently reported from a single crystal XRD study on $Li_{0.74}Ti_3O_6$ (17). A polyhedral representation of the structure, projected along [001] is presented in Fig. 6, showing the positions of the two independent octahedral framework metal atoms. Ti1 and M2, and the location of the lithium atoms in the $[2 \times 1]$ ramsdellite-type channels. A plot of the observed and calculated diffraction patterns is given in Fig. 7. A full description of the structure is presented in Ref. (17).

Polyhedral bond lengths are given in Table 6. The Ti–O bond lengths are shorter than obtained for $Li_{0.74}Ti_3O_6$, consistent with the higher ratio of Ti^{4+} to Ti^{3+}. The tetrahedral coordination of the lithium is more distorted, but not significantly so, given the large errors on the Li–O distances.

The lithium content obtained from the structure refinement is only about half of the value expected from the chemical analysis. A possible explanation is that partial hydration/oxidation of the sample had occurred. A more likely possibility is that the lithium is distributed over

TABLE 4
Comparison of Ramsdellite-Related Phases in Li_2O–Ti_2O_3–TiO_2–H_2O System

Phase	Cation atom fractions			Unit cell composition[a]	Unit cell parameters				Space group	Ref.	Comments
	[Li]	[Ti^{3+}]	[Ti^{4+}]		a (Å)	b (Å)	c (Å)	γ (°)			
$Li_{0.5}TiO_2$	0.33	0.33	0.33	Li_2 [Ti_4O_8]	5.036(1)	9.638(10)	2.948(1)		*Pbnm*	16	Ti^{3+}-containing ramsdellite
$Li_{0.16}TiO_2$	0.14	0.14	0.72	$Li_{0.64}$ [Ti_4O_8]	4.979(1)	9.561(1)	2.955(1)		*Pbnm*	4	Partial oxidation of $Li_{0.5}TiO_2$
TiO_2 (R)	0	0	1.0	[Ti_4O_8]	4.902(1)	9.459(1)	2.958(1)		*Pbnm*	4	Full oxidation/leaching of $Li_{0.5}TiO_2$
$Li_2Ti_3O_7$	0.4	0	0.6	$Li_{1.7}$ [$Ti_{3.4}Li_{0.6}O_8$]	5.016(3)	9.543(5)	2.945(2)		*Pbnm*	10	Ramsdellite-type
$H_2Ti_3O_7$	0	0	0.6	$H_{1.7}$ [$Ti_{3.4}H_{0.6}O_8$]	4.6745(4)	9.7689(6)	2.9212(2)		*Pbnm*	5	H^+-exchanged $Li_2Ti_3O_7$
TiO_2 (rutile)	0	0	1.0	[Ti_2O_4]	4.594(3)	4.594(3)	2.959(2)		*P*42/*mnm*	5	From heating $H_2Ti_3O_7$
$Li_{0.74}Ti_3O_6$	0.2	0.2	0.6	$Li_{1.5}$ [Ti_6O_{12}]	4.937(1)	14.120(1)	2.949(1)	92.69(1)	*A*112/*m*	17	Ramsdellite-rutile intergrowth
$Li_{0.86}Ti_{2.94}O_6$	0.23	0.16	0.61	$Li_{1.6}$ [$Ti_{5.9}Li_{0.1}O_{12}$]	4.9067(2)	14.107(1)	2.9525(1)	92.234(3)	*A*112/*m*	This work	Ramsdellite-rutile intergrowth
$Li_{0.38}Ti_{2.94}O_6$	0.11	0.04	0.85	$Li_{0.8}$ [$Ti_{5.9}Li_{0.1}O_{12}$]	4.7535(6)	14.147(1)	2.9572(2)	91.844(4)	*A*112/*m*	This work	8 day oxidation of $Li_{0.86}Ti_{2.94}O_6$
$Li_{0.3}Ti_{2.94}O_6$	0.09	0.02	0.89	$Li_{0.5}$ [$Ti_{5.9}Li_{0.1}O_{12}$]	4.5968(8)	14.378(2)	2.9255(4)	90.0	*A*112/*m*	This work	1 month oxidation of $Li_{0.86}Ti_{2.94}O_6$

[a]Octahedral framework given in square brackets.

a number of minor sites in the ramsdellite channels as reported for $Li_2Ti_3O_7$ (12).

Hydration/Oxidation of Intergrowth Phase

The intergrowth sample $Li_{0.86}Ti_{2.94}O_6$ underwent extensive reaction with air over a period of one month, as evidenced by the large changes in cell parameters given in Table 3, and the low analyzed Ti_2O_3 value of 1.5 wt%. The PXRD pattern, shown in Fig. 5, is metrically orthorhombic.

TABLE 5
Refinement Results for 1:1 Intergrowth Phase Using Powder Neutron Data

Preparation: 14.5 mole% Li_2O, 1100°C, $fO_2 = 10^{-16.7}$ atm
Composition: $Li_{0.98}Ti_{2.88}O_6$
Unit Cell: *A*112/*m*, $a = 4.8948(3)$, $b = 14.101(1)$, $c = 2.9531(2)$ Å, $\gamma = 92.146(3)°$
Refinement: $\lambda = 1.3717$ Å, $2\theta = 8$–$143°$, 336 reflections, 32 variables $R_{wp} = 0.074$, $R_B = 0.041$

Atom	x	y	z	B (Å^2)	Site occupancy
Ti1	0	0	0	0.5(1)	Ti
M2	0.478(1)	0.3450(4)	0	0.9(1)	0.93Ti + 0.07Li
Li	0.06(1)	0.220(4)	0	2.0(2)	0.20(3) Li
O(1)	0.7000(6)	0.2272(2)	0	0.32(5)	
O(2)	0.3051(6)	0.0974(3)	0	0.78(6)	
O(3)	0.1855(4)	0.4330(2)	0	0.66(5)	

However it was not possible to describe the intergrowth structure in an orthorhombic space group consistent with the observed systematic absences. Retention of monoclinic symmetry, *A*2/*m*, as in the unreacted sample, led to a successful refinement of the reacted sample. The atomic coordinates from the refinement of the unreacted intergrowth phase in Table 5 were used as starting coordinates for Rietveld refinement of the PXRD data. $LiOH \cdot H_2O$ was included as a second phase, with the structural parameters taken from Ref. (26). Only the profile parameters and cell dimensions were refined for $LiOH \cdot H_2O$. The refinement converged at relatively high values of $R_{wp} = 0.20$ and $R_B = 0.10$.

A difference Fourier map showed large peaks in octahedral sites in the ramsdellite-type channels. Atoms in these

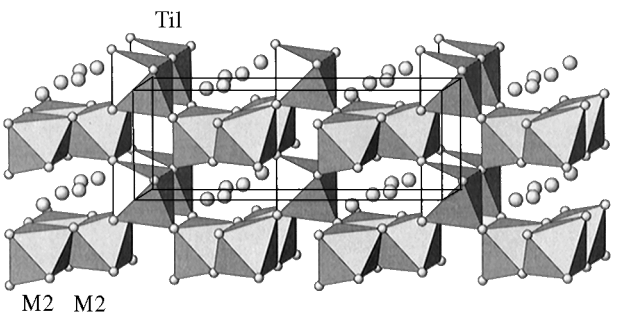

FIG. 6. Polyhedral representation of the 1:1 intergrowth structure, projected along [001]. Large open circles represent lithium atoms.

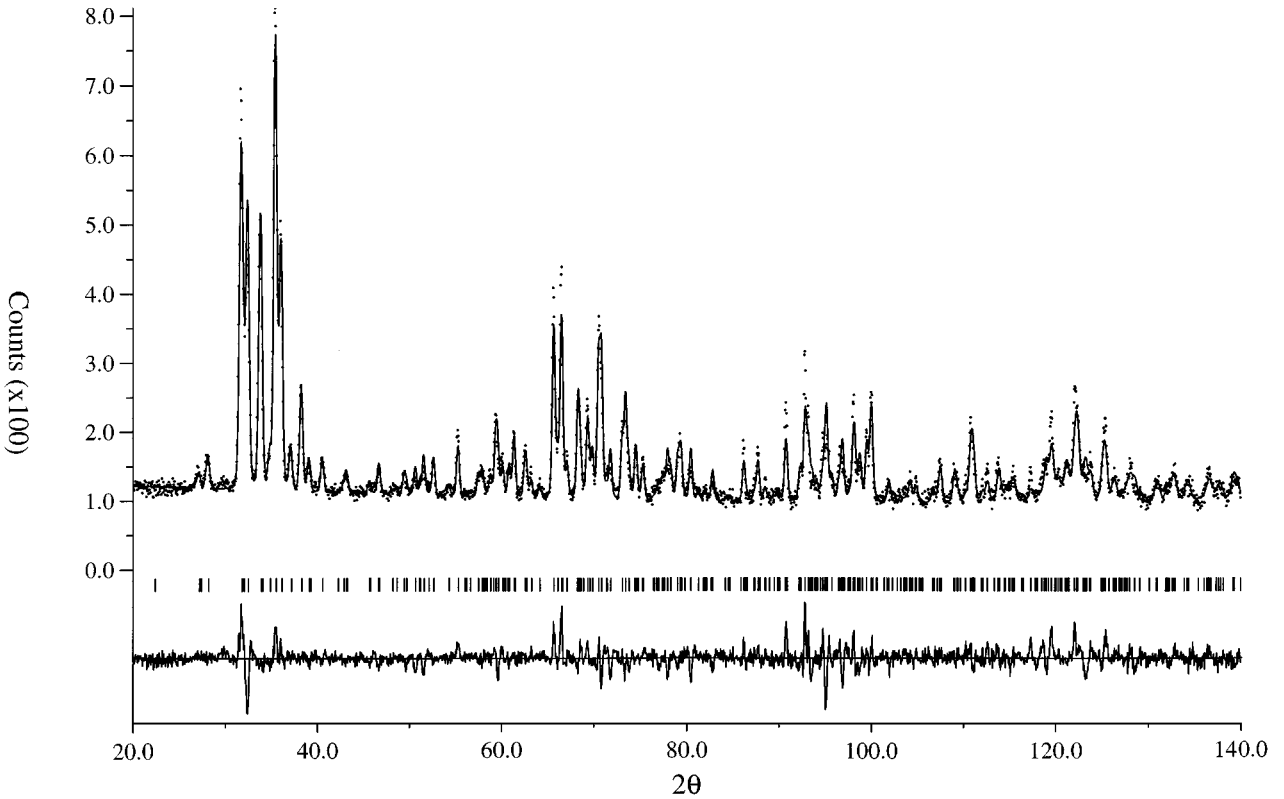

FIG. 7. Observed (dots), calculated (line), and difference plots from Rietveld refinement of neutron diffraction data for the 1:1 rutile-ramsdellite intergrowth structure of $Li_{0.98}Ti_{2.88}O_6$.

sites share octahedral faces with the Ti(2) atoms in the ramsdellite-type double chains. The scattering in the new site was too strong to be lithium and was assigned as titanium, Ti(3). The site occupancy of Ti(3) was linked in the refinement to that of Ti(2) to avoid the physically unrealistic situation of strings of face-shared octahedra with very short Ti(2)–Ti(3) separations. The refinement was continued with the inclusion of Ti(3), converging at $R_{wp} = 0.16$, $R_B = 0.045$ for the reacted intergrowth phase and $R_B = 0.078$ for $LiOH \cdot H_2O$. The refined wt% $LiOH \cdot H_2O$ was 8.7(3)%. This corresponds to over 60% of the lithium in the intergrowth structure being converted to well-crystallized $LiOH.H_2O$. With the disordering of the relatively heavy titanium atoms in the ramsdellite-type channels, it was not possible, using the PXRD data, to confirm whether any residual lithium remained in the channels. Based on the quantitative XRD phase analysis, the composition of the oxidized intergrowth phase is $Li_{0.3}Ti_{2.94}O_6$.

TABLE 6
Polyhedral Bond Lengths (Å) for Intergrowth Phases

$Li_{0.98}Ti_{2.88}O_6$ Freshly prepared		$Li_{0.86}Ti_{2.94}O_6$ after 1 month reaction with air	
Ti1–O3 (×4)	1.958(2)	Ti1–O3 (×4)	1.96(1)
Ti1–O2 (×2)	2.066(3)	Ti1–O2 (×2)	2.04(1)
⟨Ti1–O⟩	1.995	⟨Ti1–O⟩	1.99
M2–O3	1.856(6)	Ti2–O3	1.89(2)
M2–O2 (×2)	1.952(6)	Ti2–O1	1.93(2)
M2–O1 (×2)	2.008(4)	Ti2–O2 (×2)	1.94(1)
M2–O1	2.011(4)	Ti2–O1 (×2)	1.98(1)
⟨M2–O⟩	1.965	⟨Ti2–O⟩	1.94
Li–O1	1.75(5)	Ti3–O3	1.94(3)
Li–O2	2.07(5)	Ti3–O1 (×2)	1.95(1)
Li–O1 (×2)	2.05(3)	Ti3–O1	2.01(2)
		Ti3–O2 (×2)	2.38(2)
⟨Li–O⟩	1.98	⟨Ti3–O⟩	2.10

The results from the Rietveld refinement are summarized in Table 7. Approximately 20% of the titanium atoms originally in the Ti(2) sites in the ramsdellite-type octahedral chains have diffused into the channels during the reaction with air. A similar situation occurs when $Li_2Ti_3O_7$ is converted to $H_2Ti_3O_7$ by proton exchange, as reported by Le Bail and Fourquet (5). Dehydration of $H_2Ti_3O_7$ gives rise to an intermediate phase in which the titanium atoms are completely disordered over the octahedral sites in both the octahedral chains and the channels of the ramsdellite-type structure.

TABLE 7
Rietveld Refinement Results (XRD) for Hydrated/Oxidized Intergrowth Phase

Preparation:	12.8 mole% Li_2O sample, ball-milled, exposed to air for 1 month
Composition:	$Li_{0.3}Ti_{2.94}O_6$
Unit cell:	$A112/m$, $a = 4.5980(2)$, $b = 14.3816(7)$, $c = 2.9266(1)$Å, $\gamma = 90.00$
Refinement:	$2\theta = 15$–$125°$, 192 reflections, 34 variables $R_{wp} = 0.160$, $R_B = 0.046$
Second phase:	$LiOH \cdot H_2O$, $R_B = 0.077$, wt% = 8.8(3)

Atom	x	y	z	B (Å^2)	Site occupancy
Ti(1)	0	0	0	1.1(2)	1.0
Ti(2)	0.488(1)	0.3414(4)	0	0.8(1)	0.800(6)
Ti(3)	0.146(3)	0.315(1)	0	0.8(1)	0.200(6)
O(1)	0.708(2)	0.227(1)	0	1.1(1)	
O(2)	0.284(2)	0.108(1)	0	1.1(1)	
O(3)	0.212(2)	0.439(1)	0	1.1(1)	

The hydration/oxidation reaction results in a rotation of the octahedral chains about their corner linkages. This brings about a flattening of the (001) layers of oxygen atoms, giving a closer approach to hexagonal closest-packing. Polyhedral bond lengths in the reacted intergrowth phase are compared with equivalent distances in the unreacted intergrowth phase in Table 6.

(0kl)r CS Structures

Electron diffraction is a powerful technique for characterizing families of crystallographic shear structures derived from a parent structure. By alignment of the appropriate zone axis, the orientation of the CS planes and their separation, Dsp, can be measured directly off the electron diffraction patterns. Also, by observing which parent subcell reflections are split in the ED patterns, the CS displacement vector can be established. This vector describes the displacement of one block of parent structure relative to another across the CS planes. The combination of CS plane orientation, Dsp, and displacement vector allow idealized models to be constructed for the structures of the CS phases. These can be used as starting models in refinement of diffraction data to establish the local relaxations of atoms in the real structures. An ambiguity exists in relation to the displacement vector due to the fact that lattice vectors can be added to the CS vector without changing the diffraction characteristics. However this ambiguity can normally be resolved by a structure refinement. Usually the correct displacement vector is the shortest vector consistent with the diffraction characteristics.

In the case of the $(0kl)_r$ CS phases, the orientations of the CS planes all lie in the $[100]_r$ zone. Typical electron diffraction patterns are shown in Figs. 3 and 4. The ED patterns showed characteristic "crosses" of superlattice reflections, corresponding to microtwinning. As the CS plane orientation swings around closer to $(021)_r$, the microtwinning becomes less pronounced, with the ED patterns often showing a dominant twin individual.

From the splitting of the rutile subcell reflections, the CS displacement vector is established as $1/2\,[0\text{–}11]_r$ (or a vector related by a lattice displacement as discussed above). This is the same vector that operates in the well-known $(121)_r$–$(132)_r$ families of rutile-derived CS planes (27); it is also the vector found for $(020)_r$ high-temperature CS planes in the Fe_2O_3–TiO_2 system (25). Operation of this vector on the rutile structure leaves the oxygen framework unchanged (in the ideal hexagonal closest-packed representation) and results in a displacement of titanium atoms into octahedral interstitial sites.

Although the CS plane orientation and Dsp can be measured off ED patterns, it requires painstaking efforts to locate and orient the correct zone. Unless many zone axis patterns can be located for each sample, there is doubt that the observations represent the statistical average of the range of orientations and spacings in the sample. A quicker and more representative analysis of the average structure in each sample can be obtained from careful measurements of superlattice peak positions in PXRD patterns.

Expressions were developed to calculate the $(0kl)_r$ CS plane orientation and the separation between the CS planes, Dsp, from the positions of the central and satellite peaks in the PXRD pattern. For example, using second-order satellites the expressions are:

$$\mathrm{Dsp} = 3/\sqrt{2} \cdot \{(d^*_{-2})^2 + (d^*_2)^2 - 2(d^*_0)^2\}^{-0.5}$$

$$\cos\alpha = \{2.25 \cdot (\mathrm{Dsp}^*)^2 + (d^*_0)^2 - (d^*_{-2})^2\} \cdot \{3.\mathrm{Dsp}^* \cdot d^*_0\}^{-1},$$

where d_0, d_{-2}, and d_2 are the d-spacings for the central peak, low-angle, and high-angle second-order satellites respectively and α is the angle between the CS plane and the plane used in the calculations. The central peak will not be present for split subcell reflections, and its d-spacing has to be calculated from measurements of other, unsplit subcell reflections in the PXRD pattern.

The above expressions have been applied to the $(110)_r$ and $(101)_r$ reflections in the $(0kl)_r$ CS structures. The resulting Dsp and CS plane orientations for selected single-phase CS samples are listed in Table 8. For CS phases prepared at 1100°C, the CS plane periodicity was found to increase from about 11 Å for the $(051)_r$ CS structure at a Li_2O content of 6.5 mole% to a spacing of about 25 Å for a CS structure close to $(021)_r$ at 0.7 mole% Li_2O. At 1200°C, the conditions were more reducing, and compositions with the same Li_2O content as the 1100°C preparations gave more closely spaced CS planes at close to the same orientation. Thus with

TABLE 8
Calculated CS Plane Orientations and Spacings for $(0kl)_r$ CS Phases

Mole% Li_2O	Reaction temp. (°C)	Dsp (Å)	α (°)[a]	CS plane orientation
7.6	1200	9.5	47.6	$(051)_r$
6.5	1200	10.1	47.6	$(051)_r$
6.5	1100	10.8	47.3	$(051)_r$
5.2	1100	11.9	49.0	$(041)_r$
3.6	1200	11.6	51.2	$(031)_r$
3.6	1100	13.7	50.0	$(072)_r$
2.6	1100	15.1	51.6	$(031)_r$
2.1	1100	15.6	52.7	$(083)_r$
1.3	1100	19.7	53.7	$(052)_r$
0.7	1100	23.1	53.5	$(052)_r$

[a]Angle between the $(0kl)_r$ CS plane and $(110)_r$.

variation of temperature, reducing atmosphere, and lithium content, the CS phase region is able to adapt by varying either the CS plane orientation or the spacing between the planes, or both, giving great structural flexibility to accommodate the composition changes.

Preliminary attempts have been made to refine models for the $(0kl)_r$ CS structures by applying the Rietveld method to PXRD data. The general structure features have been confirmed. For example a representation of a $(051)_r$ CS structure obtained from refinement of PXRD data is shown in Fig. 8. However there are limitations to the application of powder profile refinements for these phases. Specifically, the satellite reflections are approximately twice as broad as the subcell reflections, due to the finite range of CS plane orientations and spacings in each sample. This requires special flexibility in the Rietveld program to deal with peak half-widths that are not a smoothly varying function of diffraction angle. Secondly the unit cells for the CS phases are relatively large, primitive, and non-centrosymmetric. There are thus many independent atoms in the asymmetric unit, and there is high pseudosymmetry in the relationships between atoms due to the underlying subcell structure. This gives rise to correlation problems in the refinement. In work in progress we are trying to circumvent these problems by growing single crystals of the CS phases.

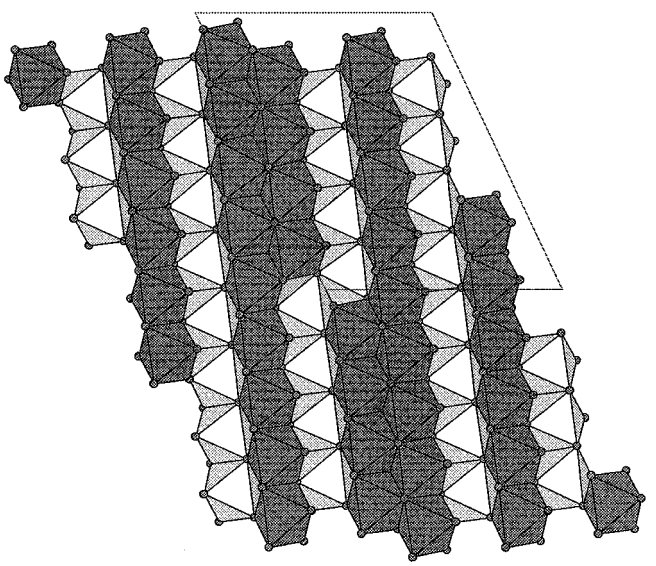

FIG. 8. Polyhedral representation of $(051)_r$ CS structure.

CONCLUSIONS

The Li_2O–TiO_{2-x} pseudobinary system displays a rich variety of phase and structure chemistry under reducing conditions. Using fixed equilibration conditions of 1100°C and $fO_2 = 10^{-16.7}$ atm, the variation of Li_2O contents between 0.7 and 30 mole% gives rise to a ramsdellite-type phase, a 1:1 ramsdellite:rutile intergrowth phase, and a family of $(0kl)_r$ rutile-derived crystallographic shear structures, with CS plane orientations swinging from $(051)_r$ to near $(021)_r$ with decrease in lithium content. Decreasing the reducing conditions was found to destabilize the CS structures relative to a new Li-anatase phase containing 4 mole% Li_2O.

An *ab initio* structure determination was made on a ramsdellite:rutile intergrowth phase, $Li_{0.98}Ti_{2.88}O_6$, using PXRD data, and the structure was refined using neutron powder data. The results are in agreement with an independent determination of the structure using single crystal XRD data (17). The intergrowth phase reacted readily with air, undergoing both oxidation of Ti^{3+} to Ti^{4+}, and hydroxylation of lithium in the structure to form $LiOH \cdot H_2O$. The reactions with air were quantified using weight gain experiments and Ti^{3+} analyses. A Rietveld refinement made on an extensively reacted sample, $Li_{0.3}Ti_{2.94}O_6$, showed that the removal of lithium from the structure was accompanied by partial disordering of titanium into the channels of the ramsdellite part of the structure and rotation of the octahedral chains about their corner linkages. Further work is required to refine the structure of the $(0kl)_r$ CS phases and to characterize structurally the lithium containing high-temperature anatase phase.

The incorporation of lithium into a number of different titanate structures under reducing conditions is likely to make the use of lithium compounds unacceptable as catalysts for the char reduction of ilmenite. The formation of lithium-containing reduced rutile phases would lead to the consumption of the expensive lithium additive and a decrease in the quality of the upgraded product.

ACKNOWLEDGMENTS

We would like to thank Margaret Elcombe and Brett Hunter, from the Australian Nuclear Science and Technology Organisation, for collecting the neutron diffraction data. Thanks also to Cheryl Mclnnes for performing the trivalent titanium analyses.

REFERENCES

1. T. Takahashi *in* "Superionic Conductors," (G. D. Mahan and W. L. Roth, Eds.), p. 389. Plenum, New York, 1976.
2. T. Ohzuku, A. Ueda, and N. Yamamoto, *J. Electrochem Soc.* **142,** 1431 (1995).
3. D. C. Johnston, *J. Low Temp. Phys.* **25,** 145 (1976).
4. J. Akimoto, Y. Gotoh, N. Nonose, T. Kumagai, K. Aoki, and H. Takei, *J. Solid State Chem.* **113,** 27 (1994).
5. A. Le Bail and J. L. Fourquet, *Mater. Res. Bull.* **27,** 75 (1992).
6. R. G. Becher, R. G. Canning, B. A. Goodheart, and S. Uusna, *Proc. Aus. IMM* **214,** 21 (1965).
7. B. P. Mohanty and K. A. Smith, *Trans. IMM, Sect. C* **102,** C163 (1993).
8. G. Izquierdo and A. R. West, *Mater. Res. Bull.* **15,** 1655 (1980).
9. J. C. Mikkelsen, Jr., *J. Am. Ceram. Soc.* **63,** 331 (1980).
10. B. Morosin and J. C. Mikkelsen Jr., *Acta Crystallogr. Sect.* **B 35,** 798 (1979).
11. A. M. Bystrom, *Acta Chem. Scand.* **3,** 163 (1949).
12. I. Abrahams, P. G. Bruce, W. I. F. David, and A. R. West, *J. Solid State Chem.* **78,** 170 (1989).
13. P. Strobel, F. le Cras, and M. Anne, *J. Solid State Chem.* **124,** 83 (1996).
14. A. Deschanvres, B. Raveau, and Z. Sekkal, *Mater. Res. Bull.* **6,** 699 (1971).
15. J. Akimoto, Y. Gotoh, K. Kawaguchi, and Y. Oosawa, *J. Solid State Chem.* **96,** 446 (1992).
16. J. Akimoto, Y. Gotoh, M. Sohma, K. Kawaguchi, and Y. Oosawa, *J. Solid State Chem.* **110,** 150 (1994).
17. J. Akimoto, Y. Gotoh, and Y. Oosawa, *J. Solid State Chem.* **129,** 7 (1997).
18. H. M. Rietveld, *J. Appl. Crystallogr.* **2,** 65 (1969).
19. R. J. Hill and C. J. Howard, *J. Appl. Crystallogr.* **18,** 173 (1985).
20. D. B. Wiles and R. A. Young, *J. Appl. Crystallogr.* **14,** 149 (1981).
21. G. Cagliotti, A. Paoletti, and F. P. Ricci, *Nucl. Instrum.* **3,** 223 (1958).
22. "International Tables for X-ray Crystallography," Vol. IV. Kynoch Press, Birmingham, UK (1974).
23. J. W. Visser, *J. Appl. Crystallogr.* **2,** 89 (1969).
24. G. M. Sheldrick, "SHELX-76, Program for Crystal Structure Determination." University of Cambridge, UK, 1976.
25. L. A. Bursill, D. J. Netherway, and I. E. Grey, *Nature* **272,** 405 (1978).
26. N. W. Alcock, *Acta Crystallogr. Sect.* **B 27,** 1682 (1971).
27. D. K. Philp and L. A. Bursill, *J. Solid State Chem.* **10,** 357 (1974).